

Heat Pipe Bending Effect on Cooling Effectiveness in Electrical Machines

Han Zhao, Xiaochen Zhang, *Member, IEEE*, Jing Li, *Senior Member, IEEE*, Huanran Wang, Fengyu Zhang, *Member, IEEE*, He Zhang, *Senior Member, IEEE*, Xiaorui Zhu, David Gerada, *Senior Member, IEEE*

Abstract—Heat pipes (HPs) are being extensively explored in motor cooling scenarios for enhanced cooling capacity. HPs are commonly bent to adapt to the compact structure of electrical machines, whereas the bending effect on motor cooling effectiveness still requires further investigation. This article analytically and experimentally studies the effect of the bending process, including bending angle and bending radius, on HP thermal properties. Cooling density is defined and derived to analyze the tradeoff between HP thermal performance and additional volume due to HP installation. Practical guidelines for feasible HP bending solutions under different space constraints are provided to achieve a higher cooling density. Finally, the HP bending effect on motor cooling effectiveness under various cooling methods is quantitatively evaluated through a validated thermal model based on a stator-winding assembly. The bending process can degrade the HP equivalent thermal conductivity by up to 76%, thus leading to a temperature difference of 4.8K under liquid cooling conditions.

Index Terms—Additional volume, bending process, cooling density, cooling effectiveness, electrical machines, experimental investigation, heat pipe, thermal analysis, thermal model.

I. INTRODUCTION

DUE to the global trend toward transportation electrification, high power density (kW/kg or kW/L) electrical machines are at the center of the electrified concept, which results in higher loss densities and requires enhanced cooling systems [1-3]. In this case, the efficient cooling technique is a significant enabler for improving the performance metrics beyond the current state of the art. Whilst, the implemented temperature reduction is directly beneficial for active material saving and reliability

promotion [4, 5].

Based on the phase change principle, the heat pipe (HP) presents outstanding thermal properties, i.e., very high thermal conductivity at a small volume and lightweight. Therefore, HPs are being widely applied in motor cooling systems with remarkable cooling performance validated through prototyping and testing [6-10]. During the design and implementation of motor cooling systems, HPs are often bent to adapt to the compact structure of high-power density motors. Fig. 1 illustrates some typical bent HP applications in electrical machines [11-13]. In these cases, the main heat source of the motor is the winding module, while the coolant is generally located externally, e.g., ambient air or liquid jacket in the housing. There is a long and curved cooling path between the heat source and the heat sink, which limits heat transfer and dissipation. Thereby, bent HPs are commonly adopted to achieve a shorter cooling path and lower thermal resistance.

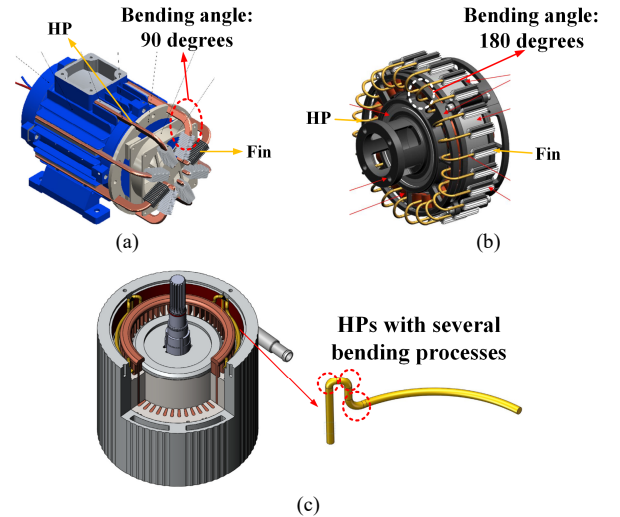


Fig. 1. Bent HPs with different bending angles applied in electrical machines. (a) 90° [11]. (b) 180° [12]. (c) Multi-bent HPs [13].

However, studies in the field of thermodynamics and mechanics have confirmed that the bending process degrades the HP thermal performance, thus reducing cooling benefits [14-17]. The main reason lies in that the wick structure is torn away from the copper shell by machining and the internal channel is deformed, which blocks the vapor flow and backflow of the working medium, as presented in Fig. 2. Most of the existing studies in electrical machines only focus on the structural design and implementation of the motor

This work was supported by Ministry of Science & Technology under National Key R&D Program of China under Grant 2021YFE0108600, Ningbo Key Technology Research and Development Programme under Grant 2021Z035, and the Key International Cooperation of National Natural Science Foundation of China under Grant 51920105011. (*Corresponding author: Xiaochen Zhang.*)

Xiaochen Zhang is with the Advanced Electric Drive Centre, Yongjiang Laboratory, Ningbo 315202, China, and the Key Laboratory of More Electric Aircraft Technology of Zhejiang Province, University of Nottingham Ningbo China, Ningbo 315100, China (email: Xiaochen.Zhang@nottingham.edu.cn).

Han Zhao, Jing Li, Huanran Wang, He Zhang and Xiaorui Zhu are with the Key Laboratory of More Electric Aircraft Technology of Zhejiang Province, University of Nottingham Ningbo China, Ningbo 315100, China (email: sgxhz1@nottingham.edu.cn; Jing.Li@nottingham.edu.cn; sgxhw2@nottingham.edu.cn; He.Zhang@nottingham.edu.cn; ssyxz8@nottingham.edu.cn).

Fengyu Zhang and David Gerada are with Power Electronics, Machines and Control Group, University of Nottingham, Nottingham NG7 2RD, U.K. (email: fengyu.zhang1@nottingham.ac.uk; David.Gerada@nottingham.ac.uk).

cooling structures based on HPs, while ignoring the negative impact of the HP bending process on its own thermal performance and also motor cooling effectiveness. Hence, few publications carry out quantitative studies on this topic and practical guidelines for the promotion of bent HPs in electrical machines are necessary, but still lacking for engineers.

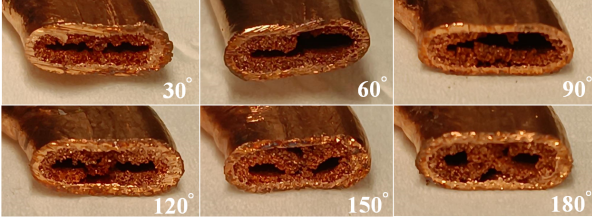


Fig. 2. Destruction of the HP internal structure during the bending process.

This study aims to fill the above knowledge gaps and the main contributions of this paper are summarized as follows:

1) The analytical model for bent HP is derived and validated by experimental results. The negative impact of the bending process, including the bending angle and the bending radius, on HP thermal properties is analytically and experimentally studied.

2) Cooling density is defined and derived to characterize the tradeoff between HP thermal conductivity and additional volume, coupled with practical guidelines provided to achieve a higher cooling density under different space constraints.

3) The bending effect on motor cooling effectiveness is quantitatively evaluated by a validated 3-D thermal model with common cooling methods.

The remainder of this article is organized as follows. Section II briefly introduces the HP working principle and derives the analytical model of bent HP. In Section III, experimental investigation is conducted to quantify the bending effect on HP thermal performance and validate the above model. Section IV defines and derives the cooling density, together with discussions on feasible HP bending solutions. In Section V, a 3-D thermal model is developed and validated to evaluate the HP bending effect on motor cooling effectiveness. Finally, a conclusion is drawn in Section VI.

II. THERMAL MODEL OF HP

The copper-water HP with sintered wick structure is commonly the preferred choice in motor cooling scenarios [18, 19]. Therefore, it is adopted in this study and its detailed parameters are listed in Table I.

TABLE I
PARAMETERS OF THE HPs USED IN THIS STUDY

Parameters	Value	Parameters	Value
Shell material	Copper	Working medium	Water
Length	170 mm	Thickness	3 mm
Width	8 mm	Shell thickness	0.4 mm
Wick thickness	0.3 mm	Porosity of wick structure	0.7
Wick structure	Sintered wick structure (Copper powder)		
Bending position	HP center		

A copper-water HP with sintered wick structure commonly

consists of a hollow sealed copper shell, a sintered wick structure, and an internal vapor space, together with a small amount of working medium contained in the chamber, as shown in Fig. 3. The HP is based on the phase transition principle, with working medium from the liquid to vapor state and vice versa. The operating medium evaporates into vapor after absorbing heat in the evaporator section. The resulting vapor is driven by high pressure to flow through the adiabatic section into the condenser section, where it condenses into liquid again and releases a large amount of heat. The condensed liquid is pumped back to the evaporator section through the capillary force generated by the wick structure to complete a whole phase change cycle.

Based on the working principle of phase transition and HP structure, the heat transfer in the HP can be divided into the following three parts: (i) heat conduction through the copper shell; (ii) heat conduction through the wick structure; and (iii) phase change heat transfer in the vapor space. Fig. 3 presents a simplified thermal model of an HP, where thermal resistances in the model correspond to the above heat transfer process. It is assumed that there is a uniform temperature distribution in the evaporator and condenser sections.

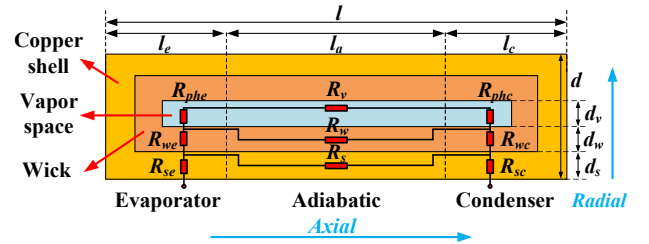


Fig. 3. Thermal model of an HP.

The thermal model of the HP is established as follows, and all related symbols are defined in Table II [20, 21]. The conductive thermal resistances in copper shell are composed of radial (R_{se} and R_{sc}) and axial (R_s) heat conduction, which are given by:

$$R_{se} = \frac{d_s}{\lambda_s \cdot 2\omega l_e} \quad R_{sc} = \frac{d_s}{\lambda_s \cdot 2\omega l_c} \quad (1)$$

$$R_s = \frac{l_{eff}}{\lambda_s \cdot 2\omega d_s}$$

$$l_{eff} = l_a + 0.5l_e + 0.5l_c$$

Similarly, the conductive thermal resistances in wick structure include radial (R_{we} and R_{wc}) and axial (R_w) heat conduction, which can be calculated by:

$$R_{we} = \frac{d_w}{\lambda_w \cdot 2(\omega - 2d_s)l_e} \quad R_{wc} = \frac{d_w}{\lambda_w \cdot 2(\omega - 2d_s)l_c} \quad (2)$$

$$R_w = \frac{l_{eff}}{\lambda_w \cdot 2(\omega - 2d_s)d_w}$$

The wick structure is a composite of sintered copper powder and working medium, which can be represented by a homogeneous material. The Chaudary and Bhandari model based on parallel method (λ_{pa}) and series method (λ_{se}) is adopted to estimate the thermal conductivity of such a homogeneous material [22], which is given by

$$\begin{aligned}\lambda_w &= \lambda_{pa}^n \cdot \lambda_{se}^{1-n} \\ \lambda_{pa} &= \varepsilon \cdot \lambda_m + (1 - \varepsilon) \cdot \lambda_s \\ \lambda_{se} &= \frac{\lambda_s \lambda_m}{\varepsilon \cdot \lambda_s + (1 - \varepsilon) \cdot \lambda_m}\end{aligned}\quad (3)$$

where the weighting factor n is usually between 0.8 and 0.9, and the value in this study is determined to be 0.8.

Additionally, the thermal resistances in the vapor space can be divided into phase change in the evaporator and condenser sections (R_{phe} and R_{phc}), and vapor flow in the vapor chamber (R_v), formalized as [20]:

$$R_{phe} = \frac{R_g T_g^2 \sqrt{2\pi R_g T_g}}{P_v h^2 \cdot 2(d_v + w - 2d_s - 2d_w) l_e} \quad (4)$$

$$R_{phc} = \frac{R_g T_g^2 \sqrt{2\pi R_g T_g}}{P_v h^2 \cdot 2(d_v + w - 2d_s - 2d_w) l_c}$$

$$R_v = \frac{R_g T_g^2 \Delta P_v}{Q P_v h} \quad \Delta P_v = \frac{8\mu_v Q l_{eff}}{\pi \rho_v A_v d_h^2 h} \quad d_h = \frac{2A_l}{C_l} \quad (5)$$

The HP bending process could narrow the internal vapor space and thus hinder the vapor flow. Two critical factors during the bending process are considered to be closely related to the HP thermal performance, i.e., bending angle α and bending radius r , which are described in Fig. 4. When the vapor flow through the bending section, there is an additional vapor pressure drop generated by hydraulic loss, which can be empirically evaluated by [23]:

$$\begin{aligned}\Delta P_b &= \xi \frac{v^2}{2g} \\ \xi &= \left[0.131 + 0.159 \left(\frac{d}{r} \right)^{3.5} \right] \cdot \frac{\alpha}{90^\circ}\end{aligned}\quad (6)$$

Therefore, the thermal resistance of vapor flow can be transformed into the following form:

$$R_v = \frac{R_g T_g^2 (\Delta P_v + \Delta P_b)}{Q P_v h} \quad (7)$$

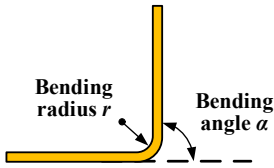


Fig. 4. Schematic of bending angle and bending radius of HP.

Since the thermal resistances of axial heat transfer in the copper shell (R_s) and wick structure (R_w) are much greater than that in parallel, thereby they are ignored in this study. Moreover, the thermal resistances of the phase change (R_{phe} and R_{phc}) are far less than the conductive thermal resistances in copper shell and wick structure, so they can also be ignored. Finally, the HP thermal resistance can be simplified into the sum of thermal resistances of the following three parts: (i) the radial heat conduction in copper shell R_{cons} ; (ii) the radial heat conduction in wick structure R_{comw} ; and (iii) vapor flow in the vapor space R_v . Additionally, the HP equivalent thermal conductivity can be also calculated as follows:

$$\begin{aligned}R_{HP} &= R_{cons} + R_{comw} + R_v \\ &= R_{se} + R_{sc} + R_{we} + R_{wc} + R_v \\ \lambda_{HP} &= \frac{l_{eff}}{R_{HP} \cdot A} = \frac{l_{eff}}{R_{HP} \cdot w \cdot d}\end{aligned}\quad (8)$$

TABLE II
NOMENCLATURE

Symbol	Concept
l_e	HP evaporator length
l_a	HP adiabatic length
l_c	HP condenser length
l_{eff}	HP equivalent length
l	HP total length
d_s	Thickness of copper shell
d_w	Thickness of wick structure
d_v	Thickness of vapor space
d_h	Hydraulic diameter of the wick structure
d	HP thickness
w	HP width
A	HP cross-sectional area
A_v	Cross-sectional area of the vapor space
A_l	Cross-sectional area of the liquid channel
C_l	Wetted perimeter of the liquid channel
λ_{HP}	HP equivalent thermal conductivity
λ_s	Thermal conductivity of shell
λ_w	Thermal conductivity of wick
λ_m	Thermal conductivity of working medium
ε	Porosity of HP wick structure
R_g	Gas constant of vapor
T_g	Vapor temperature
P_v	Vapor pressure
ρ_v	Vapor density
h	Latent heat of working medium
μ_v	Kinetic viscosity of vapor
v	Vapor flow velocity
g	Gravitational acceleration
r	HP bending radius
α	HP bending angle
ΔP_v	Vapor pressure drop
ΔP_b	Additional vapor pressure drop due to HP bending process
Q	Heat flux through the HP

III. EXPERIMENTAL INVESTIGATION

A. Experimental Setup

To validate the above HP numerical model, the HP thermal properties at various bending angles and bending radii are experimentally measured in this Section. A dedicated experimental setup based on the steady-state heat flow method is established for thermal tests, as shown in Fig. 5. The prepared specimen to be tested is affixed to the test bench with a clamp-on bench vise. The specimen is powered by an adjustable DC power supply and the input power is measured by a power meter (YOKOGAWA WT333E). To provide a uniform cooling condition, an electric fan with large fan blades is employed and placed directly opposite the specimen. The wind velocity measured by an anemometer (OMEGA

HHF144) is constant at 1.5 m/s. Moreover, the temperature variation and distribution along the specimen are monitored by thermal loggers (Pico TC-08), and then recorded in a laptop for further data processing and analysis.

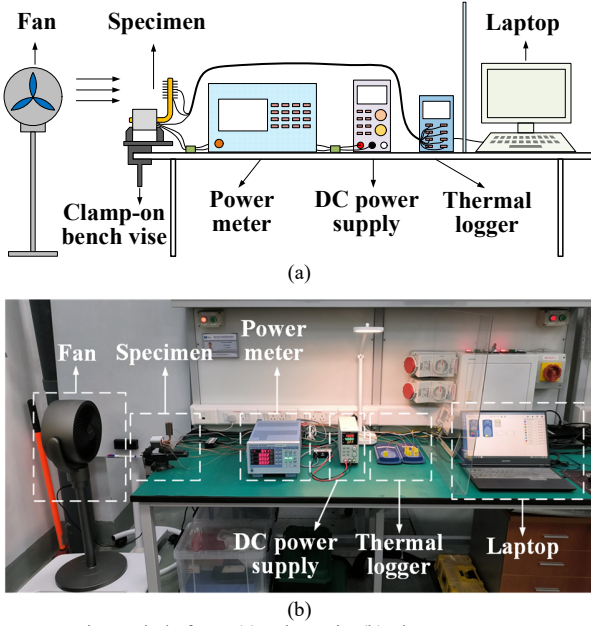


Fig. 5. Experimental platform. (a) Schematic. (b) Photo.

B. PTCHE-based Specimen Preparation

The positive temperature coefficient heating element (PTCHE), also known as self-regulating heater, is adopted as the heat source for the experimental specimen due to its advantages of the rapid warm-up, accurate temperature maintenance at fixed input voltage, absence of thermostats and overtemperature protection capability [24], as presented in Fig. 6(a). Compared to copper windings, the introduction of the PTCHE facilitates the specimen preparation and thermal test from the following three aspects: (i) small volume and timesaving for the preparation of large numbers of specimens, (ii) more precise affixation of thermocouples, thus beneficial for accurate measurement of temperature distribution along the specimen, (iii) a shorter duration before thermal equilibrium, which guarantees higher time efficiency for multiple groups of tests. The detailed parameters of the PTCHE are listed in Table III.

TABLE III
PARAMETERS OF THE PTCHE APPLIED IN THIS STUDY

Parameters	Value	Parameters	Value
Input DC voltage	24 V	Length	60mm
Steady-state temperature	110°C	Width	21mm
Temperature deviation	± 10°C	Thickness	5mm

Fig. 6(b) sketches the structure of the PTCHE-based specimen. The PTCHE and aluminum fin are attached to both ends of the HP as the heat source and the heat sink, respectively. The length of the fin is chosen to match the PTCHE, as the HP presents favorable thermal performance when the length of the evaporator section approaches the condenser section [25]. To increase the contact area and

enhance the heat conduction, a type of 92% micronized diamond powder added thermal compound (IC diamond) with a high equivalent thermal conductivity of 2000 W/m·K is applied on the contact interfaces between the PTCHE, fin and HP. Additionally, thermally conductive silica gel is used as an adhesive at both ends of the contact interface to bond them together for a more reliable connection. Finally, the entire specimen is wrapped with multi-layer thermal insulation material (Nitrile rubber) except for the fin to minimize heat losses. To obtain a detailed temperature profile along the specimen, a total of nine K-type thermocouples are affixed uniformly to different sections of the specimen by cyanoacrylate adhesive, where E_1 , E_2 and E_3 are located at the evaporator section, C_1 , C_2 and C_3 are attached to the condenser section, and F_1 , F_2 and F_3 are employed at the fin surface, respectively. Thermocouples E_1 , E_2 , E_3 , C_1 , C_2 and C_3 are located on the centerline of the HP to ensure accurate temperature measurement, as detailed in Fig. 6(c).

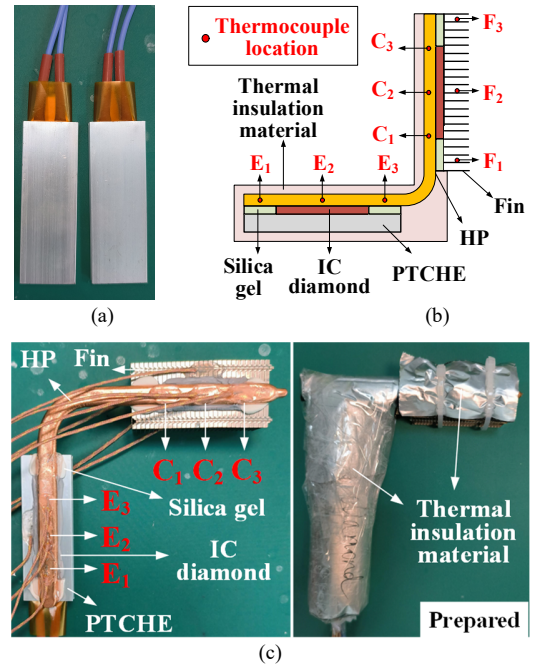


Fig. 6. PTCHE-based specimen. (a) PTCHE. (b) Sketch of the specimen preparation. (c) Photos of the specimen preparation.

To fully evaluate the bending effect on HP thermal performance, a set of PTCHE-based specimens is prepared based on the above processing method, where HPs are bent at bending angles of 0°, 30°, 60°, 90°, 120°, 150°, 180° and bending radii of 12.6 mm, 15.3 mm, 18.3 mm, 21.5 mm, 24.2 mm. The selection of bending radius depends on the fabrication process that can be provided by the supplier. The prepared specimens are presented in Fig. 7.

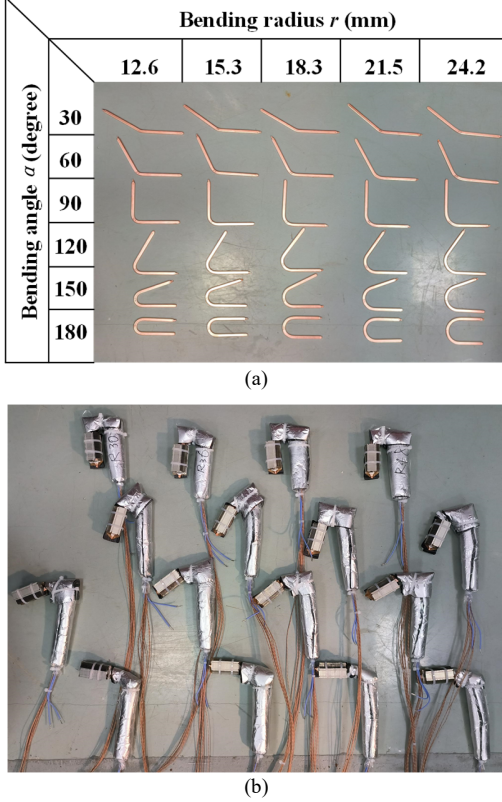


Fig. 7. Specimen preparation. (a) HPs with different bending angles and radii. (b) Part of the prepared specimens.

C. Data Processing

The HP thermal performance is characterized by its thermal resistance R_{HP} , given by:

$$R_{HP} = \frac{\Delta T}{P} = \frac{T_e - T_c}{P} \quad (9)$$

$$T_e = \frac{E_1 + E_2 + E_3}{3} \quad T_c = \frac{C_1 + C_2 + C_3}{3}$$

where P is the heat load fed into the specimen, T_e and T_c are average temperatures of the evaporator and condenser sections. Consequently, the HP equivalent thermal conductivity can be finally calculated by:

$$\lambda = \frac{l}{R_{HP}S} \quad (10)$$

where S is the HP cross-sectional area and l is the HP equivalent length, i.e., the center-to-center distance between the evaporator and condenser sections.

Additionally, the convective heat transfer coefficient of the fin can be calculated as:

$$h = \frac{P}{A \cdot \Delta T_f} \quad (11)$$

where A is the overall surface area of the fin, and ΔT_f is the temperature difference between the fin and ambient air, given by:

$$\Delta T_f = T_f - T_0 = \frac{T_{F1} + T_{F2} + T_{F3}}{3} - T_0 \quad (12)$$

where T_f is the average temperature of the fin surface and T_0 is the ambient temperature.

D. Results and Analyses

During the experiments, the temperature data is sampled and logged once a second. When the temperature variation within 5 minutes is smaller than 0.2K, thermal equilibrium is considered to be reached and the sensors data are recorded.

To distinctly demonstrate the bending effect on HP thermal properties, the variation rate V is defined to characterize the change of HP equivalent thermal conductivity in percentage, given by:

$$V = \frac{\lambda_{\max} - \lambda_{\min}}{\lambda_{\max}} \times 100\% \quad (13)$$

where λ_{\max} and λ_{\min} are the maximum and minimum value of the HP equivalent thermal conductivity at each bending angle or bending radius.

Fig. 8 illustrates the test results of HP equivalent thermal conductivities at different bending angles and bending radii. It can be found that the HP thermal performance deteriorates significantly with the increase of the bending angle, i.e., a slight decrease by 18.9% within 90° while a sharp degradation by 75.2% above 90°, as illustrated in Fig. 8(a). A greater impact of bending angle can be observed clearly with smaller bending radius, where the variation rate V declines from 75.2% ($r=12.6$ mm) to 53.9% ($r=24.2$ mm). As for the bending radius influence, the HP thermal performance gradually improves with increasing bending radius, i.e., smaller effect within 90° (V is less than 10%) while more significant influence over 90° (46% at 180°).

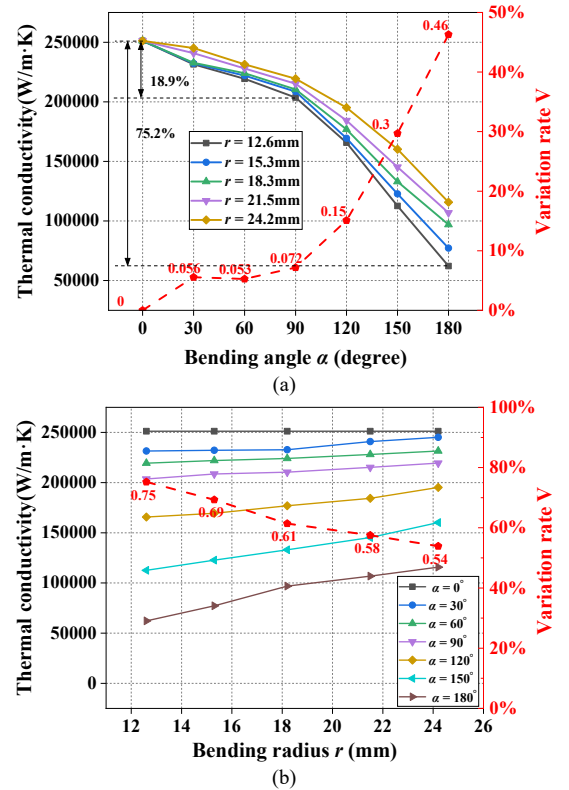


Fig. 8. HP equivalent thermal conductivities at various bending angles and bending radii. (a) Bending angle. (b) Bending radius.

Based on the above results and analyses, the following brief

conclusions can be drawn.

1) When the bending angle exceeds 90° , the bending effect becomes greater, including both bending angle and radius.

2) The HP thermal performance is more affected by the bending angle than the bending radius.

3) The influence of bending angle increases slightly with the decrease of bending radius, while the effect of bending radius enhances significantly with the increase of bending angle.

The HP equivalent thermal conductivities at various bending angles and bending radii obtained by the experiment are further compared with analytical results for validation, as presented in Fig. 9. The maximum deviation between them is within 15%, which verifies the analytical model in Section II.

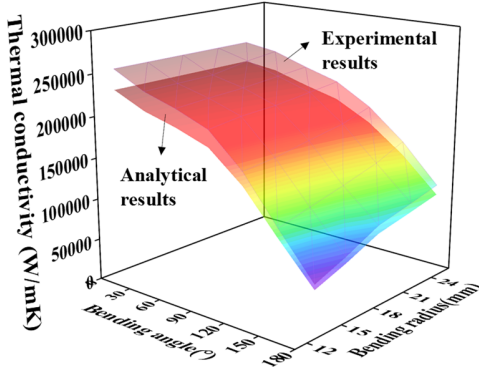


Fig. 9. Comparison between experimental results and analytical results.

Furthermore, the heat load measured by the power meter is 27.5 W and the total surface area of the fin is 0.0285 m^2 , coupled with an average temperature difference of 35K between the fin and ambient air. Thereby the convective heat transfer coefficient of the fin at a wind speed of 1.5 m/s can be calculated according to (11):

$$h = \frac{P}{A \cdot \Delta T_f} = \frac{27.5}{0.0285 \times 35} = 27.6 \text{ W/m}^2 \cdot \text{K} \quad (14)$$

IV. TRADEOFF BETWEEN HP THERMAL PERFORMANCE AND ADDITIONAL VOLUME

In motor cooling systems, HPs are generally bent to adapt to the curved cooling path and reduce additional volume, which refers to the extra space occupied by HP incorporation. On the other hand, the bending process has been proven to be detrimental to the HP thermal performance and even motor cooling effectiveness. Therefore, a tradeoff study between the HP thermal characteristics and additional volume is required to fully maximize the HP thermal benefits within a compact structure.

A. Additional Volume

The additional volume in an electrical machine consists of axial and radial sections, which can be illustrated in the sectional view of a motor equipped with bent HPs in Fig. 10. To simplify the derivation, the following assumptions are initially made in this study: (i) only the effect of bending angle is considered and bending radius is ignored; (ii) HPs are mounted evenly along the circumference of the motor surface;

(iii) HPs are bent at the middle position so that the length of the HP insertion is the same as the exposed length, which results in favorable thermal characteristics [25].

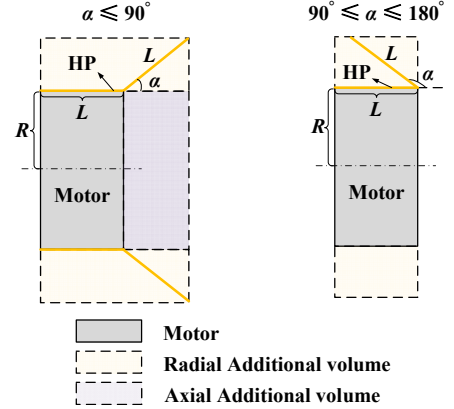


Fig. 10. Addition volume due to HP installation.

For bending angle less than 90° , the additional volume is comprised of radial and axial parts, given by:

$$\begin{aligned} V_{\alpha \leq 90^\circ} &= V_{\text{radial}} + V_{\text{axial}} = \\ &= (L + L \cos \alpha) \times [\pi (R + L \sin \alpha)^2 - \pi R^2] + L \cos \alpha \times \pi R^2 \\ &= 2\pi R L^2 \sin \alpha + \pi L^3 \sin^2 \alpha + 2\pi R L^2 \sin \alpha \cos \alpha \\ &\quad + \pi L^3 \sin^2 \alpha \cos \alpha + \pi L R^2 \cos \alpha \end{aligned} \quad (15)$$

where α is the HP bending angle, R is the motor radius and L is the length of HP insertion and exposure.

As for bending angle above 90° , only radial additional volume is generated and calculated as:

$$\begin{aligned} V_{90^\circ \leq \alpha \leq 180^\circ} &= L \times [\pi (R + L \sin \alpha)^2 - \pi R^2] \\ &= \pi L^3 \sin^2 \alpha + 2\pi R L^2 \sin \alpha \end{aligned} \quad (16)$$

In summary, the additional volume V_a can be expressed as:

$$V_a = \begin{cases} 2\pi R L^2 \sin \alpha + \pi L^3 \sin^2 \alpha \\ + 2\pi R L^2 \sin \alpha \cos \alpha \\ + \pi L^3 \sin^2 \alpha \cos \alpha \\ + \pi L R^2 \cos \alpha \\ \pi L^3 \sin^2 \alpha + 2\pi R L^2 \sin \alpha \end{cases}, \quad \begin{matrix} \alpha \in (0^\circ, 90^\circ) \\ \alpha \in (90^\circ, 180^\circ) \end{matrix} \quad (17)$$

B. Cooling Density

Generally, the HP is expected to demonstrate favorable thermal performance at a comparatively small additional volume. However, the additional volume of an electrical machine with bent HPs is contradictory to HP thermal benefits. For example, when the HP is bent at 180° , the minimum additional volume is achieved whilst the HP thermal property is also the poorest. Therefore, a new indicator, cooling density K_V , is defined in this article to characterize the tradeoff between the HP thermal characteristics and the additional volume, which is expressed as the HP equivalent thermal conductivity per unit of resulted extra space, given by:

$$K_V = \frac{\lambda_{HP}}{V_a} \quad (18)$$

It is considered to obtain a perfect tradeoff between HP

performance and motor additional volume, when cooling density K_V reaches its maximum. To facilitate derivation and calculation, the HP equivalent thermal conductivities obtained by the experiment are further fitted into a quadratic polynomial by polynomial regression, with a coefficient of determination of 0.993, which indicates a high accuracy. The expression is given by:

$$\lambda_{HP}(\alpha, r) = 2.584 \times 10^5 - 514.4\alpha - 1076r - 4.507\alpha^2 + 24.95\alpha r + 25.32r^2, \quad (19)$$

$$\alpha \in (0^\circ, 180^\circ), r \in (12\text{mm}, 25\text{mm})$$

As mentioned above, only bending angle α is considered when deriving the additional volume, so the above equation can be converted into the following form by substituting $r=12.6$ mm:

$$\lambda_{HP}(\alpha) = 268483 - 944\alpha - 0.3854\alpha^2, \alpha \in (0^\circ, 180^\circ) \quad (20)$$

Finally, the cooling density K_V can be expressed as:

$$K_V = \begin{cases} \frac{268483 - 944\alpha - 0.3854\alpha^2}{2\pi RL^2 \sin \alpha + \pi L^3 \sin^2 \alpha} + 2\pi RL^2 \sin \alpha \cos \alpha + \pi L^3 \sin^2 \alpha \cos \alpha + \pi LR^2 \cos \alpha}, & \alpha \in (0^\circ, 90^\circ) \\ \frac{268483 - 944\alpha - 0.3854\alpha^2}{\pi L^3 \sin^2 \alpha + 2\pi RL^2 \sin \alpha}}, & \alpha \in (90^\circ, 180^\circ) \end{cases} \quad (21)$$

To obtain a favorable tradeoff between HP thermal benefits and motor additional volume, the maximum value of cooling density K_V needs to be figured out. For bending angle below 90° , the maximal value of K_V depends on the motor geometry: (i) when $R \geq (1 + \sqrt{2})L$, i.e., a motor with smaller length-to-radius ratio, the maximal value appears at 90° ; (ii) when $R < (1 + \sqrt{2})L$, i.e., a motor with larger length-to-radius ratio, the maximal value is obtained at 0° . Regarding bending angle over 90° , K_V reaches its maximal value at 180° .

Combined with space constraints for motor installation, the practical guidelines for feasible HP bending angle can be finally summarized as follows based on above derivations, as illustrated in Fig. 11.

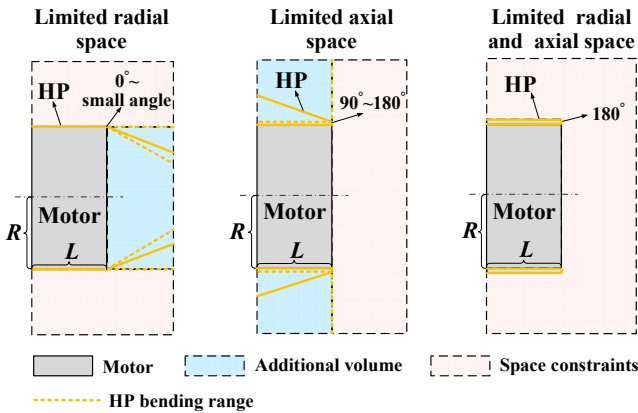


Fig. 11. Feasible solutions for HP bending angle in electrical machines under different space constraints.

1) For cases with limited radial mounting space, unbent or

slightly bent HPs are well suited for this situation, where the external cylinder of the motor is not occupied and HPs provide favorable thermal performance.

2) When faced with axial mounting space limitations, the HP bending angle can be determined between 90° and 180° according to the thermal load and cooling requirements. The right angle is ideal for high thermal load cases due to better HP thermal properties, while 180° is preferred for low thermal load scenarios to achieve a smaller additional volume.

3) Regarding space limitations in both axial and radial directions, a bending angle of 180° can be adopted for a minimum extra space or other structural implementation can be also considered based on the tradeoff between the HP performance and motor volume.

V. EVALUATION OF HP BENDING EFFECT ON MOTOR COOLING EFFECTIVENESS

A. Stator-winding Assembly

To fully evaluate the impact of HP bending process on motor cooling effectiveness, a stator-winding assembly is developed for numerical and experimental study, as detailed in Fig. 12. The copper wires are wound on a three-slot laminated stator module with slot liner used for electric insulation. An HP with a bending angle of 90° and a bending radius of 12.6 mm is inserted into the clearance between different winding layers. The same high-performance thermal compound (IC diamond) as the PTCHE-based specimen is used to fill the tiny gaps between windings and the HP to enhance heat conduction and electric insulation properties. Moreover, the fin arrangement is ensured to be identical to the PTCHE-based specimen, including material, geometry and installation method.

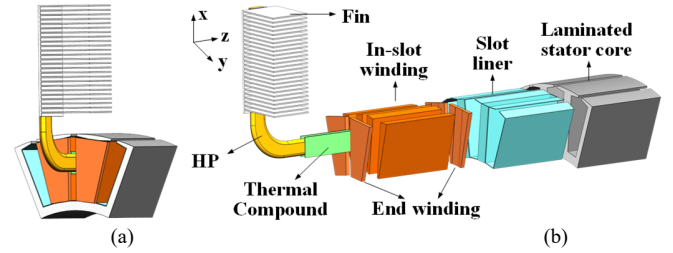


Fig. 12. Stator-winding assembly. (a) Outline. (b) Detailed view.

B. Thermal Modeling

1) *Physical Model*: A 3-D FEA thermal model is developed based on the established stator-winding assembly. To accurately quantify the temperature distribution across the thermal model, the winding module is divided into active part (in-slot winding) and end winding. The heat is transferred mainly in the axial direction (along the z-axis) in the in-slot winding, while along the y-axis in the end winding. The thermal properties of the materials involved in the thermal model are listed in Table IV.

TABLE IV
THERMAL PROPERTIES OF THE MATERIALS IN THE THERMAL MODEL

Component	Material	Thermal conductivity
-----------	----------	----------------------

		(W/m·K)
Laminated Stator core	B50A350 silicon steel sheet	$\lambda_x = \lambda_y = 43$ $\lambda_z = 1.6$
In-slot Winding	QZY-2 class F copper wire	$\lambda_x = \lambda_y = 0.433$ $\lambda_z = 400$
End winding	QZY-2 class F copper wire	$\lambda_x = \lambda_z = 0.433$ $\lambda_y = 400$
Slot liner	DMD class F insulation paper	0.3
Thermal compound	IC diamond	2000
Adhesive	Thermally conductive Silica gel	3
HP	Copper-liquid	180000 (90°, 12.6mm)
Fin	Aluminum	210

2) *Heat Source and Boundary Conditions*: The heat source and cooling condition for the thermal model are the same as the aforementioned PTCHE-based specimen. The winding module is assigned as the heat source with an identical thermal load of 27.5 W. To merely evaluate the HP bending effect on the motor cooling effectiveness, it is assumed that the heat generated is only dissipated through the cooling path including the HP and the fin. Hence, the fin surface is defined as convective boundary conditions with a convective heat transfer coefficient of $27.6 \text{ W/m}^2\cdot\text{K}$ obtained in Section III, and the remaining surfaces are specified as adiabatic boundary conditions, as presented in Fig. 13.

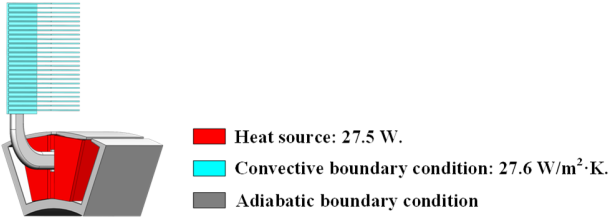


Fig. 13. Boundary conditions.

C. Numerical Results

Fig. 14 describes the steady-state temperature distribution across the thermal model, particularly in the in-slot winding and end winding region. A higher temperature is observed in the end winding region with the hotspot temperature reaching 88.6°C . Compared to the end winding, the temperature of the in-slot winding is significantly lower due to the shorter cooling path to the HP. Moreover, favorable temperature uniformity can be observed in the HP, i.e., a very small temperature difference across the HP, which indicates remarkable thermal performance.

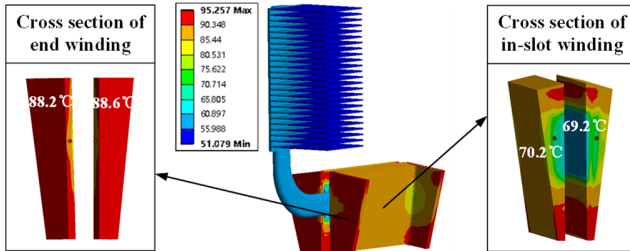
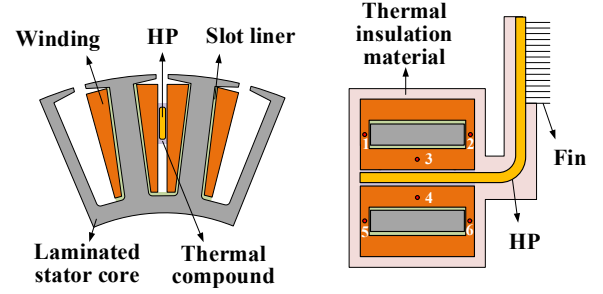


Fig. 14. Temperature distribution of the thermal model.

D. Experimental Validation

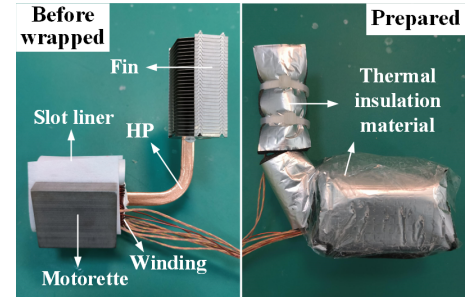
1) *Specimen Preparation*: To experimentally verify the thermal model, an experimental specimen is further processed

based on the stator-winding assembly developed in Part A, as detailed in Fig. 15. For a clear picture of the winding temperature profile, a total of six numbered thermocouples are affixed to the center of the winding section, where 3 and 4 are located at in-slot windings and the others at end windings. According to the thermal model, the entire surface of the stator-winding specimen is wrapped with multi-layer thermal insulation material (Nitrile rubber) except for the fin to minimize the heat loss. Moreover, the fin arrays of the same material and geometry are attached to the HP.



• Thermocouple location

(a)



(b)

Fig. 15. Specimen preparation based on the stator-winding assembly. (a) Sketch. (b) Prepared specimen.

2) *Comparison of Simulation and Experimental results*: The validation test is conducted on the established platform in Fig. 5 under the same heat load (27.5 W) and cooling conditions ($27.6 \text{ W/m}^2\cdot\text{K}$) as the thermal model. The comparison between calculated and measured winding temperatures is reported in Fig. 16, where the thermocouple numbers correspond to the numbering in Fig. 15(a). It can be observed that the experimental results agree well with FEA results with acceptable deviations within 4%, which confirms a good accuracy of the thermal model. The main reason for comparatively large deviations in the in-slot winding section lies in the rough thermocouple locations due to the narrow operating space in the slot.

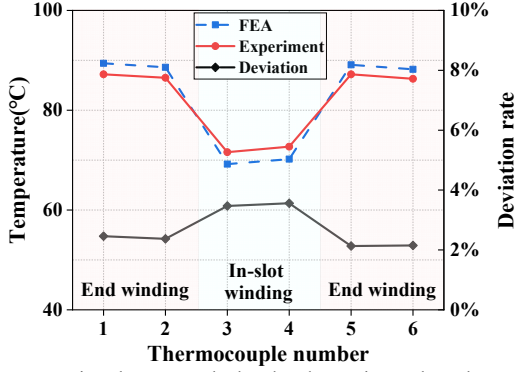


Fig. 16. Comparison between calculated and experimental results.

E. Comparative Analysis under Various Cooling Methods

Common cooling methods for electrical machines can be classified into natural convection, forced convection and liquid cooling. Their typical parameters are listed in Table V, including convective heat transfer coefficient intervals and corresponding achievable current density range [26].

TABLE V
TYPICAL PARAMETERS OF COMMON COOLING METHODS FOR ELECTRICAL MACHINES

Cooling method	Current density (A/mm ²)	Convective heat transfer coefficient (W/m ² ·K)
Natural convection	1.5-5	5-10
Forced convection	5-10	10-300
Liquid cooling	10-30	50-20000

The upper limits of the above ranges and HP equivalent thermal conductivities at different bending angles and bending radii are fed into the thermal model to evaluate the boundary of the bending effect on motor cooling effectiveness. The HP cooling performance is characterized by the average value of the steady-state temperature of the end winding which has been validated with higher accuracy. For a clearer presentation of the results, the end-winding temperature of the thermal model with unbent HP is assumed to be the base value. Hence, the temperature difference ΔT between the thermal model with bent HP and the reference value is defined as follows to describe the negative effect on motor cooling performance, given by:

$$\Delta T = T_{bent} - T_{unbent} \quad (22)$$

where T_{bent} and T_{unbent} are end-winding temperatures of the thermal model with bent and unbent HPs. Fig. 17 reports the results of ΔT under common cooling methods. An uptrend in temperature difference ΔT is observed with enhanced thermal load and cooling conditions, i.e., ΔT rises from 0.8K under natural convection to 4.8K under liquid cooling conditions, which indicates a strengthened HP bending effect on motor cooling effectiveness.

It can be inferred that the HP bending effect requires less concern for electrical machines with lower operating current densities under the passive cooling method. However, particular attention should be paid to the impact on cooling effectiveness in high power density motors under enhanced cooling conditions. In this case, a reasonable HP bending

angle can be determined according to the guidelines given in Section IV for favorable cooling effectiveness and compact structural realization.

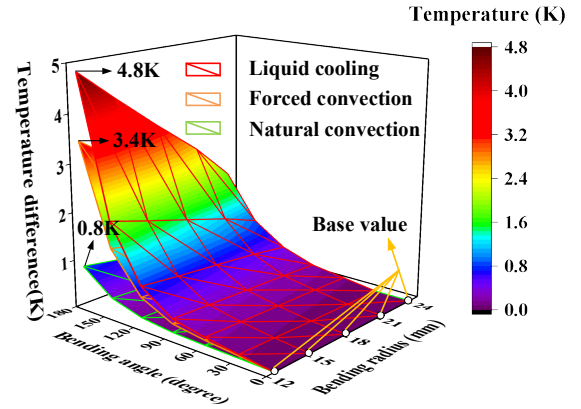


Fig. 17. Temperature difference ΔT due to HP bending effect under various cooling methods.

VI. CONCLUSION

Although HPs are being widely applied in motor cooling systems, the bending effect on motor cooling effectiveness has received less attention to date. In this article, the effect of the bending process, including the bending angle and the bending radius, on HP thermal properties has been analytically and experimentally studied. Results have shown that the HP thermal performance can be weakened by up to 76% due to the bending process, where the effect of bending angle is more significant, especially over 90°. Moreover, the cooling density has been introduced and derived to characterize the tradeoff between the HP thermal performance and additional volume. The practical guidelines for a higher cooling density under different space constraints have been provided. Unbent or slightly bent HPs are ideal for motors with radial space constraints, while HPs bent at an obtuse angle are suitable for limited axial space cases. Finally, a 3-D thermal model based on a stator-winding assembly has been developed and validated to evaluate the HP bending effect on motor cooling effectiveness. The temperature difference due to HP bending effect increases with enhanced thermal load and cooling conditions, reaching 4.8K under liquid cooling conditions.

The obtained research findings could serve as practical guidelines for electrical machines with bent HPs to enhance cooling capacity and reduce additional volume.

REFERENCES

- [1] F. Zhang *et al.*, "Back-iron extension thermal benefits for electrical machines with concentrated windings," *IEEE Transactions on Industrial Electronics*, vol. 67, no. 3, pp. 1728-1738, 2019.
- [2] P. Ramesh and N. C. Lenin, "High Power Density Electrical Machines for Electric Vehicles—Comprehensive Review Based on Material Technology," *IEEE Transactions on Magnetics*, vol. 55, no. 11, pp. 1-21, 2019, doi: 10.1109/TMAG.2019.2929145.
- [3] C. Dong, Y. Qian, Y. Zhang, and W. Zhuge, "A Review of Thermal Designs for Improving Power Density in Electrical Machines," *IEEE Transactions on Transportation Electrification*, vol. 6, no. 4, pp. 1386-1400, 2020, doi: 10.1109/te.2020.3003194.
- [4] F. Zhang *et al.*, "A Thermal Modelling Approach and Experimental Validation for an Oil Spray-Cooled Hairpin Winding Machine," *IEEE Transactions on Transportation Electrification*, 2021.

- [5] C. Liu *et al.*, "Experimental Investigation of Oil Jet Cooling in Electrical Machines with Hairpin Windings," *IEEE Transactions on Transportation Electrification*, pp. 1-1, 2022, doi: 10.1109/TTE.2022.3186947.
- [6] R. Wrobel and R. J. McGlen, "Opportunities and Challenges of Employing Heat-Pipes in Thermal Management of Electrical Machines," in *2020 International Conference on Electrical Machines (ICEM)*, 23-26 Aug. 2020, vol. 1, pp. 961-967, doi: 10.1109/ICEM49940.2020.9270932.
- [7] Z. Chen, Z. Yu, J. Fu, and B. Liu, "Study of heat pipe in motor cooling: A review," in *E3S Web of Conferences*, 2021, vol. 261: EDP Sciences.
- [8] Z. Yu, Y. Li, Y. Jing, and J. Wang, "Cooling System of Outer Rotor SPMSM for a Two-Seater All-Electric Aircraft Based on Heat Pipe Technology," *IEEE Transactions on Transportation Electrification*, pp. 1-1, 2021, doi: 10.1109/TTE.2021.3127555.
- [9] W. Le *et al.*, "A Novel Stator Cooling Structure for Yokeless and Segmented Armature Axial Flux Machine with Heat Pipe," *Energies*, vol. 14, no. 18, p. 5717, 2021.
- [10] W. Geng, T. Zhu, Q. Li, and Z. Zhang, "Windings Indirect Liquid Cooling Method for a Compact Outer-Rotor PM Starter/Generator with Concentrated Windings," *IEEE Transactions on Energy Conversion*, pp. 1-1, 2021, doi: 10.1109/TEC.2021.3084507.
- [11] N. Putra and B. Ariantara, "Electric motor thermal management system using L-shaped flat heat pipes," *Applied Thermal Engineering*, vol. 126, pp. 1156-1163, 2017, doi: 10.1016/j.applthermaleng.2017.01.090.
- [12] X. Zhang, "A Novel Cooling Technique for the Windings of High-Torque-Density Permanent Magnet Machines," 2018.
- [13] Y. Sun, S. Zhang, G. Chen, Y. Tang, and F. Liang, "Experimental and numerical investigation on a novel heat pipe based cooling strategy for permanent magnet synchronous motors," *Applied Thermal Engineering*, vol. 170, 2020, doi: 10.1016/j.applthermaleng.2020.114970.
- [14] L. Xinyu, L. Peng, H. Zhongxian, L. Tao, W. Lei, and C. Lin, "Effect of bending angle on heat transfer performance of flat heat pipe," *Energy Storage Science and Technology*, vol. 9, no. 3, p. 840, 2020.
- [15] N. Sangpab, N. Kimura, P. Terdtoon, P. Sakulchangsattajai, N. Kammuang-lue, and M. Murakami, "Combined effect of bending and flattening on heat transfer performance of cryogenic sintered-wick heat pipe," *Applied Thermal Engineering*, vol. 148, pp. 878-885, 2019.
- [16] L.-l. Jiang, Y. Tang, and M.-q. Pan, "Effects of bending on heat transfer performance of axial micro-grooved heat pipe," *Journal of Central South University*, vol. 18, no. 2, pp. 580-586, 2011.
- [17] D. D. Odhekar and D. K. Harris, "Experimental investigation of bendable heat pipes using sintered copper felt wick," in *Thermal and Thermomechanical Proceedings 10th Intersociety Conference on Phenomena in Electronics Systems, 2006. ITherm 2006.*, 2006: IEEE, pp. 8 pp-577.
- [18] A. Faghri, "Heat Pipes: Review, Opportunities and Challenges," *Frontiers in Heat Pipes*, vol. 5, no. 1, 2014, doi: 10.5098/fhp.5.1.
- [19] H. Zhao *et al.*, "A Comprehensive Review and Experimental Investigation on Heat Pipes Application in Electrical Machines," *IEEE Transactions on Transportation Electrification*, pp. 1-1, 2022, doi: 10.1109/TTE.2022.3207504.
- [20] D. Reay, R. McGlen, and P. Kew, *Heat pipes: theory, design and applications*. Butterworth-Heinemann, 2013.
- [21] M. J. Gibbons, Marco Marengo, and Tim Persoons, "A review of heat pipe technology for foldable electronic devices," *Applied Thermal Engineering*, vol. 194, p. 117088, 2021.
- [22] D. R. Chaudhary, and R.C. Bhandari, "Heat transfer through a three-phase porous medium," *Journal of Physics D: Applied Physics* 1, vol. 6, p. 815, 1968.
- [23] C. Yang *et al.*, "Fabrication and performance evaluation of flexible heat pipes for potential thermal control of foldable electronics," *Applied Thermal Engineering*, vol. 95, pp. 445-453, 2016.
- [24] Y. H. Ting, "Self-Regulating PTC Heating Systems: A New Approach for Electric Heating Appliances," *IEEE Transactions on Industry Applications*, vol. IA-8, no. 3, pp. 338-344, 1972, doi: 10.1109/TIA.1972.349765.
- [25] S. Zhang *et al.*, "Experimental study on the thermal performance of a novel ultra-thin aluminum flat heat pipe," *Renewable Energy*, vol. 135, pp. 1133-1143, 2019.
- [26] Y. Gai *et al.*, "Cooling of Automotive Traction Motors: Schemes, Examples, and Computation Methods," *IEEE Transactions on Industrial Electronics*, vol. 66, no. 3, pp. 1681-1692, 2019, doi: 10.1109/tie.2018.2835397.



Han Zhao was born in Heilongjiang, China, in 1989. He received the B.Eng. and M.Eng. degrees in electrical engineering from Harbin Institute of Technology, Harbin, China, in 2012 and 2014, respectively. He is currently working toward the Ph.D. degree within the Key Laboratory of More Electric Aircraft Technology of Zhejiang Province at the University of Nottingham Ningbo China, Ningbo, China.

His main research interests include electromagnetic and thermal analysis on electrical machines for electric propulsion applications.



Xiaochen Zhang received the master's degree from Harbin University of Science and Technology, Harbin, China, in 2006, and the Ph.D. degree from Harbin Institute of Electrical Technology, Harbin, in 2012.

He is with the Yongjiang Laboratory, and the University of Nottingham Ningbo China, Ningbo, China. His research interests include research on electromagnetic and thermal analysis on electrical machine, especially in permanent magnetic machines and high-speed machines.

Dr. Xiaochen Zhang is a fellow of Royal Aeronautical Society (FRAeS).



Jing Li received the B.Eng. and M.Sc. degrees (Hons.) from the Beijing Institute of Technology, Beijing, China, in 1999 and 2002, respectively, and the Ph.D. degree from the University of Nottingham, Nottingham, U.K., in 2010, all in electrical and electronic engineering.

She was a Research Fellow after graduation with the Power Electronics, Machine and Control Group, University of Nottingham. In 2016, she joined the University of Nottingham Ningbo China, Ningbo, China, as an Assistant Professor, where she is currently an Associate Professor with the Department of Electrical and Electronic Engineering. Her research interests include condition monitoring for motor drive systems and power distribution systems, advanced control, and design of motor drive systems.



Huanran Wang was born in Shandong, China, in 1995. He received the BSc degree in automation from the University of Jinan, Jinan, China, in 2018, and the M.Sc. degree in electrical and electronic engineering from the University of Nottingham, Nottingham, U.K., in 2019. He is currently working toward the Ph.D. degree with the University of Nottingham Ningbo China, Ningbo, China.

His current research interests include fault-tolerant control method and drive in multi-phase electric machines.



Fengyu Zhang received the B.E. degree in thermal engineering from Huazhong University of Science and Technology, Wuhan, China, in 2014, and the Ph.D. degree in electrical machines from the University of Nottingham, Nottingham, U.K., in 2019.

She is currently a Senior Research Fellow in thermal management on electrical machines within the Power Electronics, Machines and Control (PEMC) Group, University of Nottingham.

Her main research interests include high-performance motors for transport applications and their multidomain optimization.



He Zhang received the B.Eng. degree from Zhejiang University, Hangzhou, China, in 2002, and the M.Sc. and Ph.D. degrees in electrical machines from the University of Nottingham, Nottingham, U.K., in 2004 and 2009 respectively.

He worked as a Research Fellow at the University of Nottingham, where he was the Director of the BestMotion Technology Centre, Nottingham. He moved to the University of Nottingham Ningbo China, Ningbo, China, as Senior Research Fellow, in 2014, promoted to Principal Research Fellow in 2016 and Professor in 2020. He is currently the Director of the Nottingham Electrification Centre (NEC), Power Electronics, Machines and Control Research Group, University of Nottingham Ningbo China. His research interests include high-performance electric machines and drives for transport electrification.



Xiaorui Zhu was born in Shandong, China, 2001. He is currently working toward B.Eng. degree in Electrical and Electronic Engineering from the University of Nottingham Ningbo China. He is also within the Key Laboratory of More Electric Aircraft Technology of Zhejiang Province at the University of Nottingham Ningbo China, Ningbo, China.



David Gerada received the Ph.D. degree in high-speed electrical machines from University of Nottingham, Nottingham, U.K., in 2012.

From 2007 to 2016, he was with the R&D Department, Cummins, Stamford, U.K., first as an Electromagnetic Design Engineer from 2007 to 2012, and then as a Senior Electromagnetic Design Engineer and Innovation Leader from 2012 to 2016. At Cummins, he pioneered the design and development of high-speed electrical machines, transforming a challenging technology into a reliable one suitable for the transportation market, while establishing industry-wide-used metrics for such machinery. In 2016, he joined the University of Nottingham where he is currently a Principal Research Fellow, responsible for developing state-of-the-art electrical machines for future transportation which push existing technology boundaries, while propelling the new technologies to higher technology readiness levels.

Dr. Gerada is a Chartered Engineer in the U.K. and a member of the Institution of Engineering and Technology.